

Controlled Diagonal Catalyst Improves the Efficiency of Quantum Annealing

Tomohiro Hattori

¹ *Graduate School of Science and Technology, Keio University,
3-14-1 Hiyoshi, Kohoku-ku, Yokohama-shi, Kanagawa 223-8522, Japan*

Shu Tanaka^{1,2,3,4}

² *Department of Applied Physics and Physico-Informatics, Keio University,
3-14-1 Hiyoshi, Kohoku-ku, Yokohama-shi, Kanagawa 223-8522, Japan*

³ *Keio University Sustainable Quantum Artificial Intelligence Center (KSQAIC), Keio University, Tokyo 108-8345, Japan*

⁴ *Human Biology-Microbiome-Quantum Research Center (WPI-Bio2Q), Keio University, Tokyo 108-8345, Japan*

(Dated: March 20, 2025)

Quantum annealing is a promising algorithm for solving combinatorial optimization problems. It searches for the ground state of the Ising model, which corresponds to the optimal solution of a given combinatorial optimization problem. The guiding principle of quantum annealing is the adiabatic theorem in quantum mechanics, which guarantees that a system remains in the ground state of its Hamiltonian if the time evolution is sufficiently slow. According to the adiabatic theorem, the runtime required for quantum annealing to satisfy the adiabaticity scales is inverse to the square of the minimum energy gap between the ground state and the first excited state during time evolution. As a result, finding the ground state becomes significantly more difficult when the energy gap is small, creating a major bottleneck in quantum annealing. Expanding the energy gap is one strategy to improve the performance of quantum annealing; however, its implementation in actual hardware remains challenging. This study proposes a method for efficiently solving instances with small energy gaps by introducing additional local terms to the Hamiltonian and exploiting the diabatic transition remaining in the small energy gap. The proposed method achieves an approximate square speed up in time-to-solution compared to the conventional quantum annealing. In addition, we investigate the transferability of the parameters obtained with the proposed method.

I. INTRODUCTION

Quantum Annealing (QA) [1–6] is a quantum algorithm that has the potential to solve combinatorial optimization problems more efficiently than existing classical methods. In QA, the combinatorial optimization problem’s solution corresponds to the Ising model’s ground state, which the algorithm seeks to find [7, 8].

The guiding principle of QA is the adiabatic theorem in quantum mechanics [9], which describes that a system remains in its ground state during the evolution of a time-dependent Hamiltonian, provided that the evolution is sufficiently slow. The runtime required to perform QA while maintaining adiabaticity scales inversely with the square of the minimum energy gap between the ground state and the first excited state during the annealing process.

The first commercial quantum annealer [10] significantly expanded the range of applications for QA. Recently, QA has been applied to various complex problems, including combinatorial optimizations with integer variables [11–16], large-scale combinatorial optimizations [17–23], and black-box optimizations [24–31]. In addition, QA has been applied to the fields of physical simulation and computer-aided engineering [32–36].

However, hardware limitations of quantum annealers, such as decoherence, size restrictions, and energy range restrictions, hinder the availability of quantum annealers. The parameter tuning proposed in recent studies is crucial in the method of overcoming these hardware

limitations, since the limitations affect QA performance sensitively [22, 23, 37–39]. Decoherence poses significant difficulties to adiabatic time evolution. As a result, combinatorial optimization problems that require long annealing times—such as those where the QA Hamiltonian exhibits a small energy gap—are particularly difficult to solve on current hardware.

A well-known bottleneck of QA is the occurrence of perturbative crossings and quantum first-order phase transitions during the annealing process. When perturbative crossings or quantum first-order phase transitions occur, the energy gap decreases exponentially with system size, as has been analytically proven [40]. Numerous studies have been conducted to mitigate these bottlenecks [41–48].

One promising approach to overcoming these bottlenecks is to expand the energy gap. Previous studies have shown that adding an extra term, a catalyst, is crucial in achieving this expansion. A well-known example is the introduction of antiferromagnetic quantum fluctuations in the fully connected p -spin model [42], leading to an exponential increase in the energy gap.

In addition, XX -catalysts have been shown to improve the scaling of the energy gap in the Maximum Weighted Independent Set (MWIS) problem, a well-known toy model that exhibits perturbative crossings [47, 48]. Moreover, under certain conditions, diagonal catalysts—terms in the computational basis have been found to exponentially improve the energy gap scaling in the fully connected p -spin model [46].

However, implementing these approaches in existing

QA hardware remains difficult due to the non-local nature of these catalysts. In particular, non-local terms beyond ZZ -interactions and XX -interactions as catalyst terms are not yet realizable in current hardware. Therefore, exploring the potential of local catalysts is essential for practical implementations.

Shortcuts to adiabaticity (STA) [49–53] provide fast routes to the final quantum state and have the potential to drastically accelerate QA. STA introduces an additional term that forcibly cancels out diabatic transitions during time evolution, ensuring that the quantum state always follows the adiabatic path, even over short time scales.

However, formulating the STA rigorously in advance is difficult, as it requires knowledge of all eigenstates throughout the evolution. To address this, various approximate formulations of STA have been proposed [54–56], including variational approaches [57], and hardware implementations have also been investigated [58] to overcome the practical limitations of STA.

These approaches are particularly useful in gate-based quantum computing, where quantum states can be freely manipulated using unitary operations. However, implementing STA in quantum annealers remains demanding due to hardware limitations, which typically allow only homogeneous control over z -fields and x -fields. An exception is the anneal offset [59], which allows individual control of spins in a quantum annealer. Nevertheless, further research is required to fully understand and optimize the effects of anneal offsets.

The other approach that is more practical in a quantum annealer is the optimization of the annealing schedule. Optimization of the annealing schedule can reduce the time required to obtain optimal solutions [60, 61]. In the previous study, the annealing-schedule optimization improved the QA performance for the frustrated ring model, which has the perturbative crossing [60]. Also, the previous study proposes the optimization method using Bayesian optimization on a neutral-atom quantum processor for both QA and reverse annealing [61]. An optimized schedule dramatically speeds up the QA compared to QA with a linear schedule.

When performing QA with an optimized annealing schedule, the evolution of the quantum system does not strictly adhere to the adiabatic theorem in quantum mechanics. Instead, the system leverages diabatic transitions and temporarily occupies excited states during annealing, driven by the optimized annealing schedule. Consequently, the proposed method exploits the diabatic dynamics to improve the performance. However, a detailed theoretical understanding of the underlying mechanism remains incomplete.

The annealing-schedule optimization method also faces practical restrictions arising from hardware limitations. Implementing an optimized annealing schedule involving quadratic terms in the Ising Hamiltonian is particularly difficult. Additional physical qubits are necessary when embedding a densely connected Ising model onto hard-

ware with restricted connectivity. For instance, the minor embedding [62, 63] technique introduces redundant qubits to express the original dense problem graph onto the hardware topology. These interactions between the redundant qubits are strong enough to align these qubits in the same direction.

When optimizing the annealing schedule, the effects of couplers between redundant qubits must be considered. Nevertheless, the number of couplers and qubits grows quadratically with the size of the Ising model, and precise control of the annealing schedule is required. However, the precise control of the complex terms is difficult in current hardware. From this perspective, the scalability of the algorithm is inherently limited.

This study proposes a method for optimizing the annealing schedule using only linear terms of z fields. Specifically, we introduce additional longitudinal magnetic fields into the QA Hamiltonian. The schedule of these additional longitudinal magnetic fields is optimized variationally, while the annealing schedules of other terms are fixed. The proposed approach is highly practical for hardware implementation because the additional local z -fields can be realized through existing anneal-offset techniques in quantum annealers. Implementing linear z -field terms is significantly easier than incorporating quadratic z -terms, further improving the feasibility. Numerical experiments demonstrate that our proposed method solves MWIS problems faster than conventional QA with a linear annealing schedule.

II. SETTINGS

We review the quantum annealing and Maximum Weighted Independent Set, which we use as a benchmark problem with perturbative crossings. In addition, we introduce the proposed method using local magnetic fields as a catalyst.

A. Quantum annealing

The Hamiltonian of the QA is expressed as follows:

$$\mathcal{H}(s) = A(s)\mathcal{H}_q + B(s)\mathcal{H}_p, \quad 0 \leq s \leq 1, \quad (1)$$

where $A(s)$ and $B(s)$ are the annealing schedules which satisfy $A(0) \gg B(0)$ and $A(1) \ll B(1)$, and s is the elapsed time normalized by the annealing time τ , denoted as $s = t/\tau$. \mathcal{H}_q is the transverse magnetic field. \mathcal{H}_p is the Ising model whose ground state corresponds to the solution of the combinatorial optimization problem. Therefore, the ground state search for \mathcal{H}_p means solving the combinatorial optimization problem. The quantum system evolves following the Schrödinger equation. The Schrödinger equation is denoted as follows:

$$i\frac{\partial}{\partial t} |\psi(s)\rangle = \mathcal{H}(s) |\psi(s)\rangle. \quad (2)$$

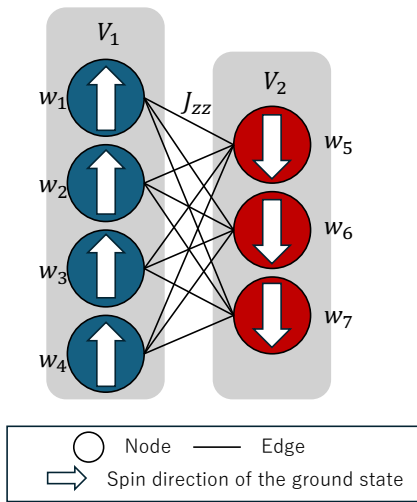


FIG. 1. Conceptual diagram of the Ising model for MWIS on $K_{4,3}$. The circles represent the nodes in $K_{4,3}$, and the black lines indicate the edges. $K_{4,3}$ consists of two subsets, with nodes depicted as dark blue and red circles, respectively. Each spin on the nodes of $K_{4,3}$ has an associated weight denoted by w_i . The white arrows represent the spin directions in the ground state of the Ising model. Each interaction on the edges in $K_{4,3}$ has a homogeneous value J_{zz} .

Here, the Planck units are used.

According to the adiabatic condition [4], the annealing time for following the instantaneous ground state is scaled as the inverse square of the minimum energy gap during QA. Therefore, the energy gap is widely exploited to measure QA properties. The energy gap $\Delta(s)$ between the ground state $|\phi_0(s)\rangle$ and the first excited state $|\phi_1(s)\rangle$ at the elapsed time s is defined as:

$$\Delta(s) = E_1(s) - E_0(s), \quad (3)$$

where $E_1(s)$ and $E_0(s)$ are the eigenenergies of $|\phi_1(s)\rangle$ and $|\phi_0(s)\rangle$, respectively.

B. Perturbative crossing in Maximum Weighted Independent Set

Under certain conditions, the energy gap closes near the end of the QA, named perturbative crossing. The perturbative crossing occurs under the condition with the small energy gap of \mathcal{H}_p between the ground state and the first excited state and the significant Hamming distance between them [40].

MWIS on a complete bipartite graph $G(V_1 + V_2, E)$ is one of the combinatorial optimization problems, where $V_1 + V_2$ and E are the sets of vertices and edges of the complete bipartite graph. The vertices of a complete bipartite graph $G(V_1 + V_2, E)$ are partitioned into two subsets, V_1 and V_2 . There are no edges between the vertices in the same subset, and all nodes have edges between the vertices in the other subset. When the number of vertices in V_1 and V_2 is expressed as $|V_1| = m$ and

$|V_2| = n$, respectively, the complete bipartite graph is expressed by $K_{m,n}$. Here, we set $m = n + 1$ to set different c_i for vertices in different subsets following the previous study [47, 48].

MWIS on the complete bipartite graph is formulated into the Ising model expressed as follows:

$$\mathcal{H}_p = \sum_{i \in V_1, V_2} (c_i J_{zz} - w_i) \sigma_i^z + \sum_{(i,j) \in E} J_{zz} \sigma_i^z \sigma_j^z, \quad (4)$$

where J_{zz} , c_i , and w_i are the weight of edges, the number of edges connected to vertex i , and the weight on vertex i , respectively and σ_i^z denotes the z -component of Pauli matrix on vertex i .

We generated 500 instances of MWIS under conditions leading to perturbative crossings. All interactions between the subsets V_1 and V_2 are set to be antiferromagnetic $J_{zz} = 1$. In this way, we treat J_{zz} as a unit of energy. Specifically, each instance was constructed with very small weights w_i , randomly assigned from a Gaussian distribution with a mean of 0 and variance $0.005/N$. Due to these small values of w_i , the energy difference between the ground state and the first excited state becomes extremely small, thereby inducing perturbative crossings. Under these conditions, the ground state and the first excited state are predominantly determined by subtle differences in the summation term $\sum_{i \in V_1, V_2} w_i s_i$.

Figure 1 shows an example of the ground state configuration of the Ising model formulated MWIS for $K_{4,3}$. Since w_i is negligible compared to J_{zz} , the antiferromagnetic interactions dominate over the local magnetic fields in determining the spin configuration. Therefore, the spin belonging to V_1 and the spin belonging to V_2 are opposite directions in the ground state, as shown in Fig. 1.

Among 500 MWIS instances, we observed two types: those with the 1 Hamming distance and those with the N Hamming distance. The ratio between the accumulated energy difference between all two-state combinations and the accumulated energy difference of the 1 Hamming distance states is a metric used to measure the difficulty of solving combinatorial optimization problems using classical methods [64, 65]. It is easy to solve for instances whose accumulated energy difference between the 1 Hamming distance states is diminutive. Since classical methods with $O(N)$ by single-spin flip make solving instances with the 1 Hamming distance easy, we focus on cases with the N Hamming distance. Also, we selected instances with a valley of the energy gap between the ground state and the first excited state about s . The selected instances are hard to solve using classical methods and QA. Therefore, MWIS on a complete bipartite graph with the N Hamming distance between the ground state and the first excited state is a crucial benchmark problem.

Figure 2 shows the energy gap $\Delta(s)$ of $\mathcal{H}(s)$ for the selected MWIS instances. $\Delta(s)$ closes at the near-final annealing time in all instances, as shown in Fig. 2 (a). Figure 2 (b) scopes $\Delta(s)$ at the near-final annealing time. In most instances, it has an energy gap that sharply

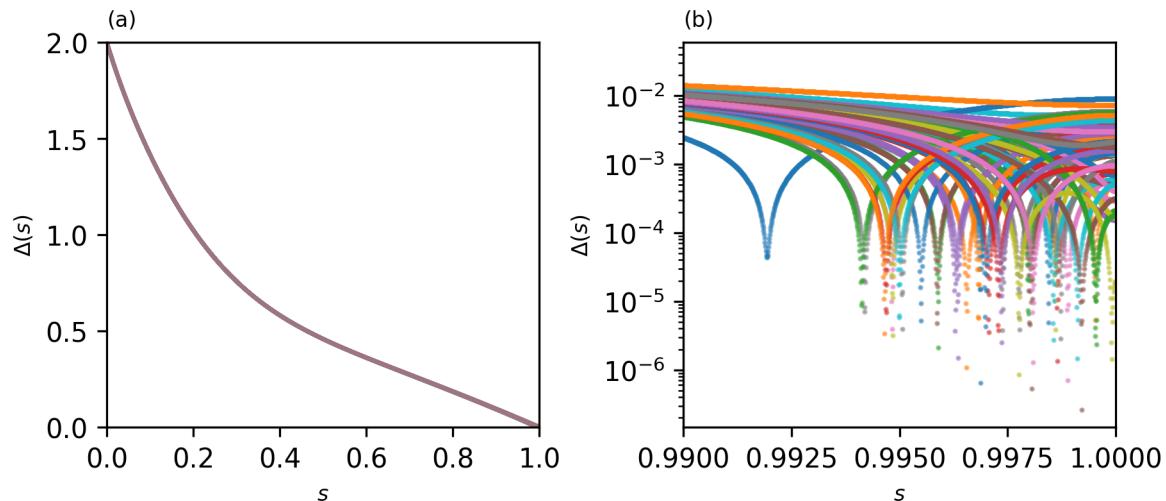


FIG. 2. (a) Energy gap $\Delta(s)$ between the ground state and the first excited state as a function of s for MWIS with the N -Hamming-distance configuration. Since the energy difference between the ground state and the first excited state in the problem Hamiltonian is extremely small, the energy gap $\Delta(s)$ closes near the end of the annealing process. (b) Energy gap $\Delta(s)$ between the ground state and the first excited state as a function of s for MWIS with the N -Hamming-distance configuration in the range $0.99 \leq s \leq 1$. The vertical axis is on a logarithmic scale. The energy gap rapidly closes near the end of the annealing process.

closes. Obtaining the ground state at the final time for these instances is difficult with conventional QA because the small energy gap allows the system to be excited to higher energy levels. We investigated the performance of the proposed method for such hard MWIS instances.

C. Proposed method

Previous studies have examined various methods for adding catalysts [42, 46–48]. The catalysts realize the exponential speed-up of QA for the specific problems. However, it is difficult to introduce the catalysts into the actual hardware because the catalysts are non-local. In this study, we add the catalyst with the linear term to investigate the potential of the local catalysts. The Hamiltonian of the QA with the catalyst is expressed as follows:

$$\mathcal{H}(s) = A(s)\mathcal{H}_q + B(s)\mathcal{H}_p + C(s)\mathcal{H}_{\text{catalyst}}, \quad (5)$$

where $C(s)$ is the annealing schedule of the catalyst restricted with $C(0) = C(1) = 0$, the $\mathcal{H}_{\text{catalyst}}$ is the diagonal catalyst, which is expressed as follows:

$$\mathcal{H}_{\text{catalyst}} = - \sum_{i=1}^N \sigma_i^z. \quad (6)$$

Since $\mathcal{H}_{\text{catalyst}}$ has only the linear term, it is easier to implement the optimized schedule into the hardware. Indeed, the restricted diagonal catalyst in hardware can be realized by using individual scheduling by local magnetic fields [66].

$C(s)$ is variationally optimized in the proposed method. In this study, to simulate the accessibility of the gradient method, we used optimal control theory [67], which was also exploited in previous studies [68, 69]. The optimal control theory enables us to numerically evaluate the gradient of the expected energy at the final time for $C(s)$ from the quantum state at the elapsed time s .

First, we define the control problem as the expected energy at the final time, which is denoted as follows:

$$\mathcal{J} = \langle \psi(1) | \mathcal{H}_p | \psi(1) \rangle. \quad (7)$$

where $|\psi(s)\rangle$ is the quantum state at the elapsed time s . To find the optimal $C(s)$, which realizes the lowest expected energy at the final time, we perform functional derivative to the control problem with $C(s)$. The results are denoted as follows:

$$\frac{\partial \mathcal{J}}{\partial C(s)} = 2\text{Im}(\langle k(s) | \mathcal{H}_{\text{catalyst}} | \psi(s) \rangle), \quad (8)$$

where $\text{Im}(\cdot)$ denotes the imaginary part, $|k(1)\rangle$ satisfies $|k(1)\rangle = \mathcal{H}_p | \psi(1) \rangle$, and $|k(s)\rangle$ is obtained by numerically solving the Schrödinger equation by using time reversal properties of the Schrödinger equation.

Using the gradient derived in Eq. (8), we iteratively update annealing schedule $C(s)$ as follows:

$$C^{(p+1)}(s) \leftarrow C^{(p)}(s) - \eta \frac{\partial \mathcal{J}}{\partial C^{(p)}(s)}, \quad (9)$$

where $C^{(p)}(s)$ is the annealing schedule repeatedly optimized p times and η is the learning rate. The number of

iterations optimizing $C(s)$ is 1000, and η is 0.01 in this study.

In the proposed method, the annealing schedules $A(s)$ and $B(s)$ are set as $A(s) = 1 - s$ and $B(s) = s$, respectively, and optimized $C(s)$ is used. The time evolution following Eq. (2) with $\mathcal{H}(s)$ written in Eq. (5) performs in our proposed method.

III. RESULTS

We numerically investigated the performance and properties of the proposed method. Also, we investigated the transferability of the optimized schedule in the proposed method. QA simulation is performed by solving the Schrödinger equation with QuTiP [70, 71]. In this study, we set $\tau = 512$, which is the long annealing time compared to $J_{zz} = 1$. However, the QA with a linear schedule cannot obtain the ground state at the final annealing time with $\tau = 512$ due to a small energy gap.

A. Performance of the proposed method

This study aims to obtain the optimal solution faster than the conventional method. However, there are trade-offs in finding the solution with a high probability in a single long run of the algorithm and running the algorithm multiple times with a shorter run time and a more negligible single-run success probability. Time-to-solution (TTS) measures the time required to find the desired probability p_d (typically $p_d = 0.99$), which can reflect the trade-off [72, 73]. Since TTS has the annealing-time dependence, we denote the TTS as $TTS(\tau)$. $TTS(\tau)$ is expressed by the equation:

$$TTS(\tau) = \tau \frac{1 - \ln(p_d)}{1 - \ln(p(\tau))}, \quad (10)$$

where $p(\tau)$ is the ground-state probability obtained by QA and we set $p_d = 0.99$ in this study. The dependence of the annealing time is shown in Appendix A.

Figure 3 shows the size scaling of TTS. TTSs of both the QA with a linear schedule and the proposed method scale exponentially about N . However, the proposed method indicates shorter TTS than the QA with a linear schedule. Table I shows the details of the fitting functions. The fitting function is calculated using the least squares method. As illustrated in Table I, the proposed method leads to square acceleration of the conventional QA since the ratio of the coefficients for N between the fitting functions is $0.85/0.46 \sim 1.8$ which means an approximate square speed up. These results show that even if the catalyst is local, it has the potential to improve QA performance.

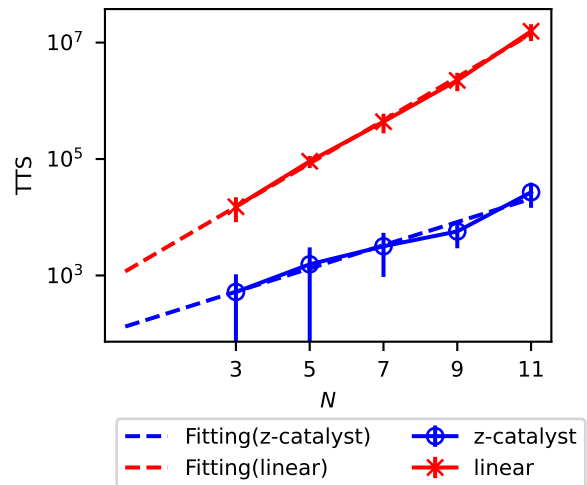


FIG. 3. Size scaling of TTS for MWIS hard instances with $\tau = 512$. The vertical axis is on a logarithmic scale. The points represent the mean TTS values for MWIS hard instances, while the error bars indicate the standard deviation. The dashed lines represent the fitting function obtained using the least squares method (see Table I).

TABLE I. TTS fitting function obtained using the least squares method. C_1 and C_2 represent constant values.

Linear schedule	Proposed method
$TTS = C_1 \exp(0.85N)$	$TTS = C_2 \exp(0.46N)$

B. Energy level population

The guiding principle of QA is the adiabatic theorem. Therefore, many previous studies aim to follow the adiabatic path [5, 52, 53, 55, 56]. However, the proposed method aims to reduce the expected energy at the final time following Eq. (7). Hence, the path to the ground state in the proposed method is not necessarily adiabatic. The diabatic path has the potential to surpass the adiabatic QA.

To investigate the dynamics of the proposed method, we numerically simulated the energy population during QA. The energy population at the l th eigenstate is denoted as follows:

$$P_l(s) = |\langle \phi_l(s) | \psi(s) \rangle|^2, \quad (11)$$

where $|\phi_l(s)\rangle$ is the l th eigenstate of $\mathcal{H}(s)$.

Figure 4 shows the result of the ground state population and the first excited state population at time t for the specific instance with $N = 11$. In Fig. 4, the dynamics of QA with linear schedule tries to follow the ground state. However, the system deviates from the ground state near the final time, where the energy gap becomes small. On the other hand, the dynamics of the proposed method deviates from the ground state earlier than those of QA with a linear schedule, and the ground state population decreases as time evolves. Finally, the

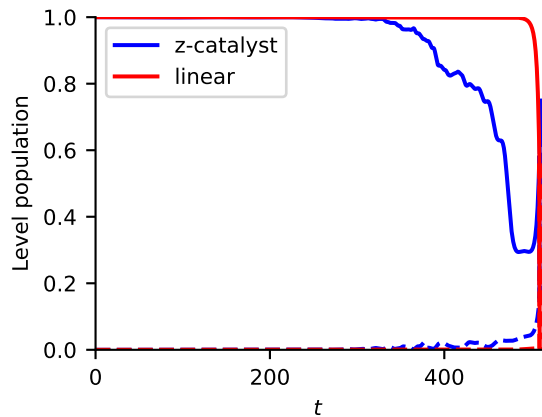


FIG. 4. Energy-level population during the time evolution for a hard MWIS instance with $N = 11$. The annealing time is set to $\tau = 512$. The blue solid line represents the ground-state population of the proposed method, while the red solid line represents the ground-state population of QA with a linear schedule. The dashed lines indicate the population of the first excited state. The color distinctions are the same as before.

population of the ground state increases when the energy gap is the smallest. Other hard MWIS instances exhibit similar energy-level population behaviour. Different from the adiabatic path, these dynamics have been investigated in the previous study [60], called diabatic QA. The proposed method realizes the diabatic QA by optimizing the schedule of only the linear terms. These results indicate that individual manipulation of the linear term is essential to shorten the solution search for hard instances. In the proposed method, fine manipulations of the quadratic terms are unnecessary. The proposed method can potentially obtain the ground state, which the QA with a linear schedule cannot do even if the annealing time increases.

C. Optimized schedule transferability

The proposed method in Section III A achieves a significantly shorter TTS than QA with a linear schedule. However, the proposed method requires optimization costs to realize the improvement of QA. Therefore, considering the time required to obtain an optimized schedule, the proposed method is not necessarily superior to the conventional approach with respect to overall computational efficiency. Thus, eliminating the schedule optimization cost is essential for the practical applicability of the proposed method.

In previous studies, parameter transferability [74–76] has been numerically investigated in the context of the Quantum Approximate Optimization Algorithm (QAOA) [2], a variational algorithm that leverages the adiabatic evolution of a quantum system as well as QA. Transferability allows the reuse of an optimized schedule

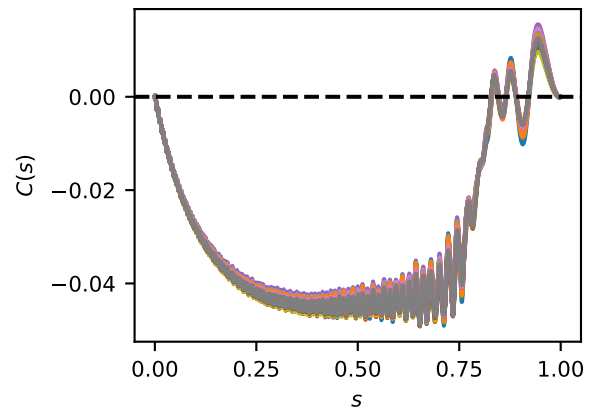


FIG. 5. Optimized schedule for MWIS hard instances with $N = 11$. The annealing time is set to $\tau = 512$ when optimizing the annealing schedule. The black dashed line represents the reference line at zero. Different colours indicate the results for different MWIS instances.

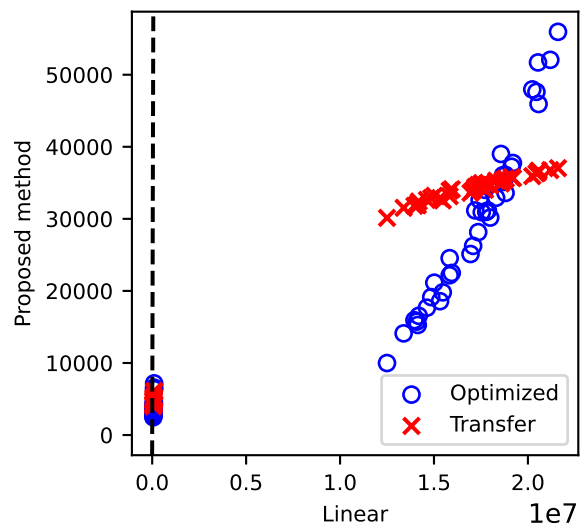


FIG. 6. TTS comparison between QA with a linear schedule and the proposed method for MWIS hard instances with $N = 11$. The annealing time is set to $\tau = 512$. The blue markers represent the proposed method with an individually optimized additional schedule. The red markers represent the proposed method with an additional schedule transferred from an arbitrarily selected MWIS hard instance. The dashed black line represents the equal TTS between the proposed method and the QA with a linear schedule.

across different problem instances, thereby circumventing the need for repetitive schedule optimization. The computational cost associated with schedule optimization can be effectively omitted if the parameters are transferable.

We investigated the transferability of the optimized schedule in the proposed method. Figure 5 illustrates the optimized schedules for different MWIS instances. The variations between these schedules are negligible com-

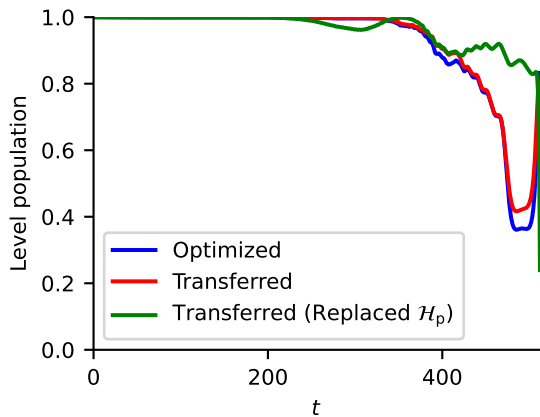


FIG. 7. Energy-level population during the time evolution for a hard MWIS instance with $N = 11$. Other hard MWIS instances exhibit similar energy-level population behaviour. The blue solid line represents the ground-state population of the proposed method, the red solid line represents the ground-state population of the proposed method with a transferred schedule, and the green solid line represents the ground-state population of the Hamiltonian in which the energy levels have been modified so that the Hamming distance between the ground state and the first excited state is 1.

pared to the overall magnitude of the annealing schedule for both the transverse field and the Ising model. This similarity suggests the optimized schedules for different MWIS instances exhibit strong structural resemblance. Therefore, these parameters are transferable across MWIS instances. The annealing time dependence of the optimized schedule is in Appendix B.

Figure 6 compares the TTS between QA with a linear schedule and the proposed method. The blue circles represent the proposed method with an individually optimized schedule $C(t)$, while the red markers indicate the proposed method using a schedule $C(t)$ transferred from an arbitrary MWIS instance. As shown in Fig. 6, the proposed method outperforms QA with a linear schedule even when using the transferred schedule. These results demonstrate the feasibility of omitting schedule optimization costs for similar MWIS instances.

In Fig. 6, the transferred schedule indicate shorter TTS than optimized schedule in some instances. The TTS difference is from the small difference of the optimized schedule shown in Fig. 5. Since the schedule optimization process in the proposed method is slightly different between MWIS instances, the degrees of convergence are different for different MWIS instances even if the same settings in the number of iterations and the learning rate.

Investigating the underlying reason for the transferability is crucial for extending these results to other combinatorial optimization problems. In MWIS instances, the energy gap near the end of QA is small. According to the adiabatic theorem in quantum mechanics, the energy gap between the ground state and the first excited

state during QA is a critical property that strongly depends on the configuration of the problem Hamiltonian.

To analyze the impact of this energy gap structure, we construct a replaced energy-level Hamiltonian in which the Hamming distance between the ground state and the first excited state is set to 1 while preserving the energy spectrum of the original Ising model for MWIS. In contrast, the original Ising model for MWIS has the N Hamming distance between these states. Using this replaced energy-level Hamiltonian, we examine the properties of schedule optimization and its transferability.

Figure 7 illustrates the instantaneous ground-state population of the proposed method for MWIS hard instances under three different scheduling conditions: an optimized schedule, a transferred schedule, and a transferred schedule applied to the replaced energy-level Hamiltonian. In Fig. 7, the ground-state population for the replaced energy-level Hamiltonian deviates significantly from that of the original Hamiltonian.

The proposed method with the optimized schedule and transferred schedule leverages adiabatic transitions during the time evolution, whereas the proposed method using the transferred schedule for replaced energy-level Hamiltonian does not effectively exploit diabatic transitions. Consequently, schedule transferability does not hold between Ising models with the same energy spectrum but the different Hamming distance between the ground state and the first excited state. Therefore, schedule transferability is influenced by the Hamming distance between the ground state and the first excited state when diabatic transitions play a significant role in QA.

These findings suggest that the performance evaluation of QA cannot be solely determined by the energy gap between the ground state and the first excited state during the annealing process.

IV. CONCLUSION AND DISCUSSION

We have investigated the effects of local diagonal catalysts on MWIS instances with a small energy gap near the final stages of QA. In particular, we focused on the potential of local diagonal catalysts by optimizing the catalyst schedule for hard instances that are challenging to solve using conventional QA. Our results demonstrate that the local diagonal catalyst significantly improves the QA performance for MWIS. The scaling analysis indicates that the proposed method achieves a quadratic speed up.

Moreover, the dynamical properties of the system play a crucial role. Diabatic transitions are essential for efficiently exploring the ground state in the proposed method. We have also examined the transferability of the catalyst schedule. Our findings reveal that, in certain cases, the catalyst schedule optimized for complex MWIS instances can be transferred to the other MWIS instances, particularly when QA with a linear schedule requires a long runtime to reach the ground state. This investigation is limited among the same number of spins.

Extensions of the transferability to the other number of spins are future work.

By investigating the replaced energy-level Hamiltonian, which preserves the energy spectrum of the original model while altering the Hamming distance, we revealed that the schedule optimization depends on both the energy levels and the Hamming distance from the ground state of the Ising model. These results suggest that the energy landscape of the Ising model plays a crucial role in diabatic QA. Therefore, the energy landscape transformation of the Ising model can be an effective strategy to reduce the cost of scheduling optimization [77–79].

ACKNOWLEDGMENTS

This work was partially supported by the Japan Society for the Promotion of Science (JSPS) KAKENHI (Grant Number JP23H05447), the Council for Science, Technology, and Innovation (CSTI) through the Cross-ministerial Strategic Innovation Promotion Program (SIP), “Promoting the application of advanced quantum technology platforms to social issues” (Funding agency: QST), Japan Science and Technology Agency (JST) (Grant Number JPMJPF2221). T. H. was supported by JST SPRING, Grant Number JPMJSP2123 and NICT Quantum Camp 2023. The computations in this work were partially performed using the facilities of the Supercomputer Center, the Institute for Solid State Physics, The University of Tokyo. S. T. wishes to express their gratitude to the World Premier International Research Center Initiative (WPI), MEXT, Japan, for their support of the Human Biology/Microbiome-Quantum Research Center (Bio2Q).

Appendix A: Annealing time dependence of time to solution

Figure 8 shows the annealing-time dependence of TTS. Figure 8 (a) shows that the TTS by QA of a linear sched-

ule is shorter than the proposed method when $\tau = 16.0$ and $N = 11$. In this condition, the system remains in its initial state, with the QA of a linear schedule, similar to uniform random sampling. Also, the behaviour of the TTS for N deviates from the exponential fitting function. According to the comparison of Fig. 8 (a), (b), (c), and (d), as the τ is longer, the performance improvement by the proposed method is more prominent. The results indicate the proposed method only works with long τ . When τ is insufficient to obtain the ground state, the system moving the local minimum is the strategy to reduce the energy. According to Eq. (7), the proposed method aims to reduce energy at the final time. Therefore, the proposed method obtains lower energy than conventional QA. That is the reason the proposed method is worse in TTS.

Appendix B: Annealing time dependence of the optimized annealing schedule

Figure 9 shows the annealing-time dependence of the optimized annealing schedule in the proposed method. Figures 9 (a)-(d) show that the optimized annealing schedule for different MWIS with $N = 11$ when $\tau = 16.0$, $\tau = 32.0$, $\tau = 100.0$ and $\tau = 256.0$, respectively. The difference of the degree of the convergence is small when the proposed method is performed with sufficient annealing time. Even if the different annealing time, the variations between these schedules are negligible compared to the overall magnitude of the annealing schedule for both the transverse field and the Ising model. Therefore, the optimized schedule transferabilities are confirmed.

-
- [1] T. Kadowaki and H. Nishimori, Quantum annealing in the transverse ising model, *Phys. Rev. E* **58**, 5355 (1998).
 - [2] E. Farhi, J. Goldstone, S. Gutmann, and M. Sipser, Quantum computation by adiabatic evolution, arXiv preprint quant-ph/0001106 (2000).
 - [3] C. C. McGeoch, *Adiabatic quantum computation and quantum annealing: Theory and practice* (Morgan & Claypool Publishers, 2014).
 - [4] S. Tanaka, R. Tamura, and B. K. Chakrabarti, *Quantum spin glasses, annealing and computation* (Cambridge University Press, 2017).
 - [5] T. Albash and D. A. Lidar, Adiabatic quantum computation, *Reviews of Modern Physics* **90**, 015002 (2018).
 - [6] B. K. Chakrabarti, H. Leschke, P. Ray, T. Shirai, and S. Tanaka, Quantum annealing and computation: challenges and perspectives, *Philosophical Transactions of the Royal Society A* **381**, 20210419 (2023).
 - [7] A. Lucas, Ising formulations of many np problems, *Frontiers in physics* **2**, 5 (2014).
 - [8] K. Tanahashi, S. Takayanagi, T. Motohashi, and S. Tanaka, Application of ising machines and a software development for ising machines, *Journal of the Physical Society of Japan* **88**, 061010 (2019).
 - [9] T. Kato, On the adiabatic theorem of quantum mechanics, *Journal of the Physical Society of Japan* **5**, 435 (1950).

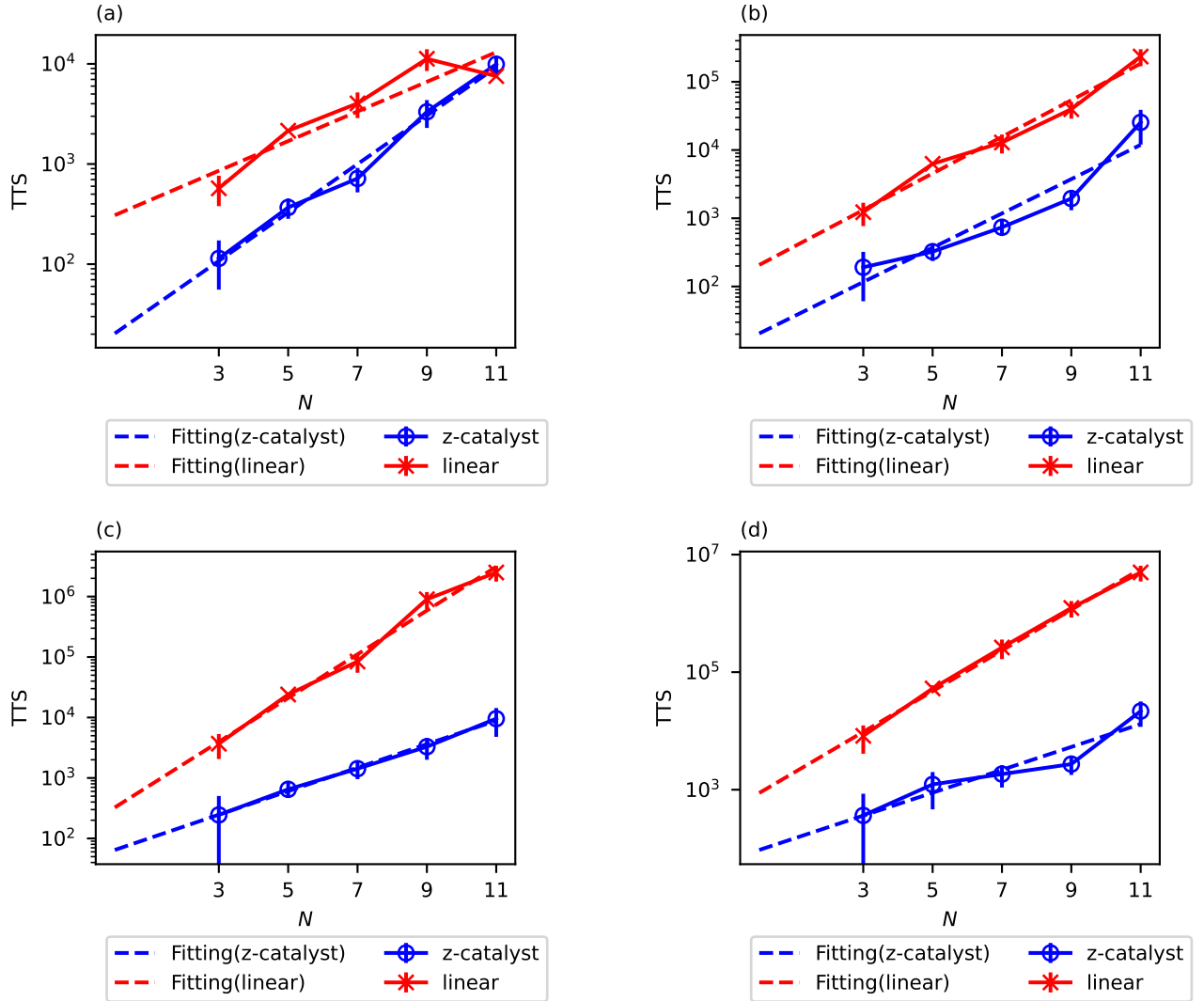


FIG. 8. Scaling of TTS with system size for MWIS hard instances. The vertical axis is on a logarithmic scale. Points represent the mean TTS values computed over MWIS hard instances, and error bars indicate standard deviations. Dashed lines represent fitting functions obtained via the least squares method. Panels show results for different annealing durations: (a) $\tau = 16$, (b) $\tau = 32$, (c) $\tau = 100$, and (d) $\tau = 256$.

- [10] M. W. Johnson, M. H. Amin, S. Gildert, T. Lanting, F. Hamze, N. Dickson, R. Harris, A. J. Berkley, J. Johansson, P. Bunyk, *et al.*, Quantum annealing with manufactured spins, *Nature* **473**, 194 (2011).
- [11] N. Chancellor, Domain wall encoding of discrete variables for quantum annealing and qaoa, *Quantum Science and Technology* **4**, 045004 (2019).
- [12] S. Okada, M. Ohzeki, and S. Taguchi, Efficient partition of integer optimization problems with one-hot encoding, *Scientific reports* **9**, 13036 (2019).
- [13] J. Chen, T. Stollenwerk, and N. Chancellor, Performance of domain-wall encoding for quantum annealing, *IEEE Transactions on Quantum Engineering* **2**, 1 (2021).
- [14] K. Tamura, T. Shirai, H. Katsura, S. Tanaka, and N. Togawa, Performance comparison of typical binary-integer encodings in an ising machine, *IEEE Access* **9**, 81032 (2021).
- [15] Y. Seki, R. Tamura, and S. Tanaka, Black-box optimization for integer-variable problems using ising machines and factorization machines, arXiv preprint arXiv:2209.01016 (2022).
- [16] S. Kikuchi, K. Takahashi, and S. Tanaka, Performance of domain-wall encoding in a digital ising machine, arXiv preprint arXiv:2410.11198 (2024).
- [17] H. Karimi and G. Rosenberg, Boosting quantum annealer performance via sample persistence, *Quantum Information Processing* **16**, 166 (2017).
- [18] H. Karimi, G. Rosenberg, and H. G. Katzgraber, Effective optimization using sample persistence: A case study on quantum annealers and various Monte Carlo optimization methods, *Phys. Rev. E* **96**, 043312 (2017), arXiv:1706.07826 [cs.DM].
- [19] S. Okada, M. Ohzeki, M. Terabe, and S. Taguchi, Improving solutions by embedding larger subproblems in

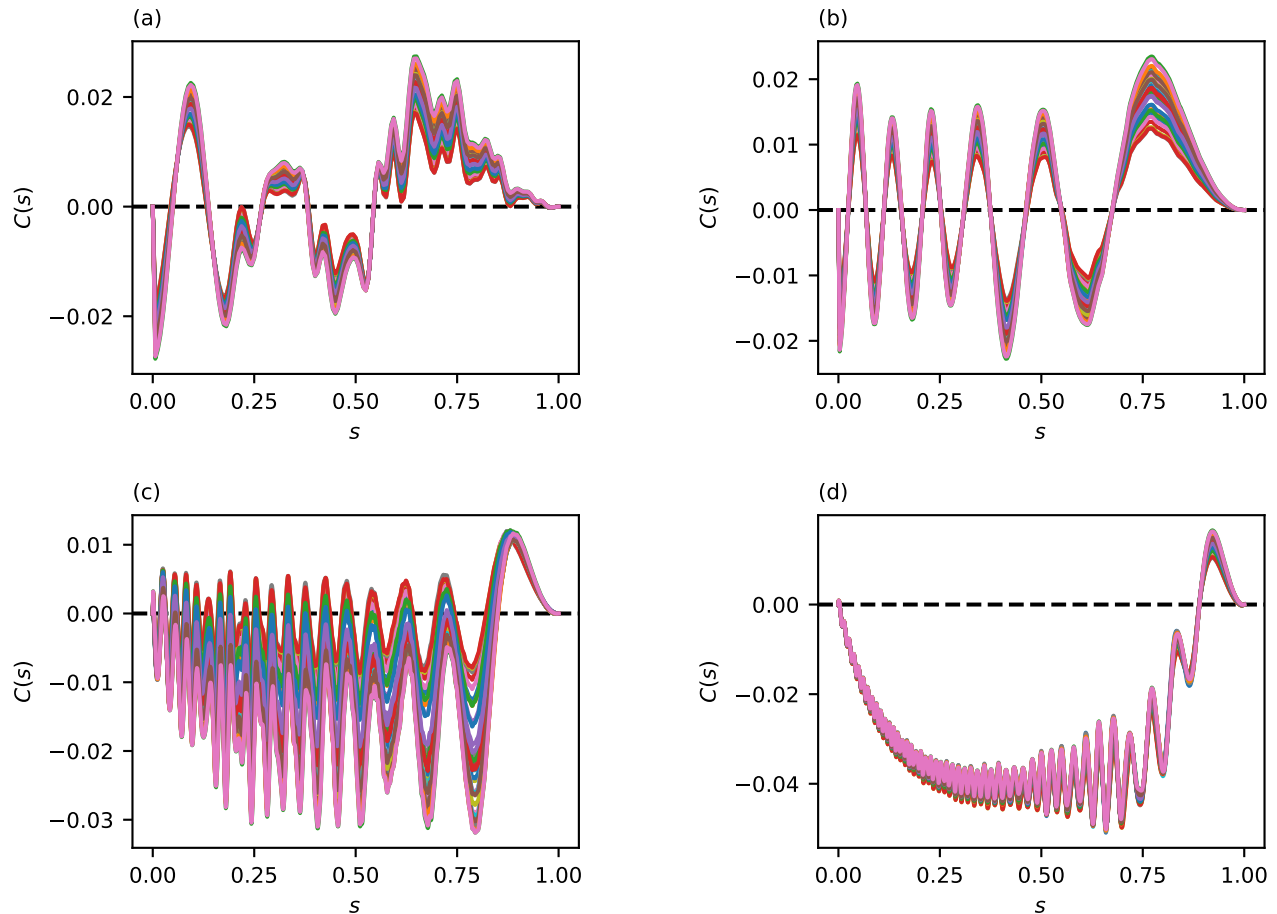


FIG. 9. Optimized schedule for MWIS hard instances with $N = 11$. The black dashed line represents the reference line at zero. Different colours indicate the results for different MWIS instances. Panels show results for different annealing durations: (a) $\tau = 16$, (b) $\tau = 32$, (c) $\tau = 100$, and (d) $\tau = 256$.

- a d-wave quantum annealer, *Scientific reports* **9**, 2098 (2019).
- [20] H. Irie, H. Liang, T. Doi, S. Gongyo, and T. Hatsuda, Hybrid quantum annealing via molecular dynamics, *Sci. Rep.* **11**, 8426 (2021).
- [21] Y. Atobe, M. Tawada, and N. Togawa, Hybrid annealing method based on subqubo model extraction with multiple solution instances, *IEEE Transactions on Computers* **71**, 2606 (2022).
- [22] S. Kikuchi, N. Togawa, and S. Tanaka, Hybrid optimization method using simulated-annealing-based ising machine and quantum annealer, *Journal of the physical society of Japan* **92**, 124002 (2023).
- [23] T. Hattori, H. Irie, T. Kadowaki, and S. Tanaka, Advantages of fixing spins in quantum annealing, *Journal of the Physical Society of Japan* **94**, 013001 (2025).
- [24] K. Kitai, J. Guo, S. Ju, S. Tanaka, K. Tsuda, J. Shiomi, and R. Tamura, Designing metamaterials with quantum annealing and factorization machines, *Phys. Rev. Res.* **2**, 013319 (2020).
- [25] T. Inoue, Y. Seki, S. Tanaka, N. Togawa, K. Ishizaki, and S. Noda, Towards optimization of photonic-crystal surface-emitting lasers via quantum annealing, *Opt. Express* **30**, 43503 (2022).
- [26] T. Matsumori, M. Taki, and T. Kadowaki, Application of qubo solver using black-box optimization to structural design for resonance avoidance, *Scientific Reports* **12**, 12143 (2022).
- [27] S. Izawa, K. Kitai, S. Tanaka, R. Tamura, and K. Tsuda, Continuous black-box optimization with an ising machine and random subspace coding, *Phys. Rev. Res.* **4**, 023062 (2022).
- [28] K. Nawa, T. Suzuki, K. Masuda, S. Tanaka, and Y. Miura, Quantum annealing optimization method for the design of barrier materials in magnetic tunnel junctions, *Phys. Rev. Appl.* **20**, 024044 (2023).
- [29] S. Kim, S.-J. Park, S. Moon, Q. Zhang, S. Hwang, S.-K. Kim, T. Luo, and E. Lee, Quantum annealing-aided design of an ultrathin-metamaterial optical diode, *Nano Convergence* **11**, 16 (2024).
- [30] J. Xiao, K. Endo, M. Muramatsu, R. Nomura, S. Moriguchi, and K. Terada, Application of factorization machine with quantum annealing to hyperparameter optimization and metamodel-based optimization in granular flow simulations, *International Journal for Numerical and Analytical Methods in Geomechanics* **48**, 3432 (2024).

- [31] K. Endo and K. Z. Takahashi, Function smoothing regularization for precision factorization machine annealing in continuous variable optimization problems, *Physical Review Research* **7**, 013149 (2025).
- [32] R. Harris, Y. Sato, A. J. Berkley, M. Reis, F. Altomare, M. Amin, K. Boothby, P. Bunyk, C. Deng, C. Enderud, *et al.*, Phase transitions in a programmable quantum spin glass simulator, *Science* **361**, 162 (2018).
- [33] A. D. King, J. Carrasquilla, J. Raymond, I. Ozfidan, E. Andriyash, A. Berkley, M. Reis, T. Lanting, R. Harris, F. Altomare, *et al.*, Observation of topological phenomena in a programmable lattice of 1,800 qubits, *Nature* **560**, 456 (2018).
- [34] R. Honda, K. Endo, T. Kaji, Y. Suzuki, Y. Matsuda, S. Tanaka, and M. Muramatsu, Development of optimization method for truss structure by quantum annealing, *Scientific reports* **14**, 13872 (2024).
- [35] K. Takagi, N. Moriya, S. Aoki, K. Endo, M. Muramatsu, and K. Fukagata, Implementation of spectral methods on ising machines: toward flow simulations on quantum annealers, *Fluid Dynamics Research* **56**, 061401 (2024).
- [36] Z. Xu, W. Shang, S. Kim, E. Lee, and T. Luo, Quantum annealing-assisted lattice optimization, *npj Computational Materials* **11**, 4 (2025).
- [37] M. H. Amin, A. D. King, J. Raymond, R. Harris, W. Bernoudy, A. J. Berkley, K. Boothby, A. Smirnov, F. Altomare, M. Babcock, *et al.*, Quantum error mitigation in quantum annealing, arXiv preprint arXiv:2311.01306 (2023).
- [38] A. Braida, S. Martiel, and I. Todinca, Tight lieb–robinson bound for approximation ratio in quantum annealing, *npj Quantum Information* **10**, 40 (2024).
- [39] T. Hattori, H. Irie, T. Kadowaki, and S. Tanaka, Impact of fixing spins in a quantum annealer with energy rescaling, arXiv preprint arXiv:2502.01008 (2025).
- [40] B. Altshuler, H. Krovi, and J. Roland, Anderson localization makes adiabatic quantum optimization fail, *Proceedings of the National Academy of Sciences* **107**, 12446 (2010).
- [41] R. D. Somma, D. Nagaj, and M. Kieferová, Quantum speedup by quantum annealing, *Phys. Rev. Lett.* **109**, 050501 (2012).
- [42] Y. Seki and H. Nishimori, Quantum annealing with antiferromagnetic fluctuations, *Phys. Rev. E* **85**, 051112 (2012).
- [43] Y. Susa, Y. Yamashiro, M. Yamamoto, and H. Nishimori, Exponential speedup of quantum annealing by inhomogeneous driving of the transverse field, *Journal of the Physical Society of Japan* **87**, 023002 (2018).
- [44] Y. Susa, Y. Yamashiro, M. Yamamoto, I. Hen, D. A. Lidar, and H. Nishimori, Quantum annealing of the p-spin model under inhomogeneous transverse field driving, *Phys. Rev. A* **98**, 042326 (2018).
- [45] J. I. Adame and P. L. McMahon, Inhomogeneous driving in quantum annealers can result in orders-of-magnitude improvements in performance, *Quantum Science and Technology* **5**, 035011 (2020).
- [46] T. Albash and M. Kowalsky, Diagonal catalysts in quantum adiabatic optimization, *Phys. Rev. A* **103**, 022608 (2021).
- [47] N. Feinstein, L. Fry-Bouriaux, S. Bose, and P. A. Warburton, Effects of xx catalysts on quantum annealing spectra with perturbative crossings, *Phys. Rev. A* **110**, 042609 (2024).
- [48] R. Ghosh, L. A. Nutricati, N. Feinstein, P. A. Warburton, and S. Bose, Exponential speed-up of quantum annealing via n-local catalysts, arXiv preprint arXiv:2409.13029 (2024).
- [49] M. Demirplak and S. A. Rice, Adiabatic population transfer with control fields, *The Journal of Physical Chemistry A* **107**, 9937 (2003).
- [50] M. Demirplak and S. A. Rice, On the consistency, extremal, and global properties of counterdiabatic fields, *The Journal of chemical physics* **129** (2008).
- [51] M. V. Berry, Transitionless quantum driving, *Journal of Physics A: Mathematical and Theoretical* **42**, 365303 (2009).
- [52] X. Chen, A. Ruschhaupt, S. Schmidt, A. del Campo, D. Guéry-Odelin, and J. G. Muga, Fast optimal frictionless atom cooling in harmonic traps: Shortcut to adiabaticity, *Phys. Rev. Lett.* **104**, 063002 (2010).
- [53] T. Hatomura, Shortcuts to adiabaticity: theoretical framework, relations between different methods, and versatile approximations, *Journal of Physics B: Atomic, Molecular and Optical Physics* **57**, 102001 (2024).
- [54] H. Saberi, T. Opatrny, K. Mølmer, and A. del Campo, Adiabatic tracking of quantum many-body dynamics, *Phys. Rev. A* **90**, 060301 (2014).
- [55] S. Campbell, G. De Chiara, M. Paternostro, G. M. Palma, and R. Fazio, Shortcut to adiabaticity in the lipkin-meshkov-glick model, *Phys. Rev. Lett.* **114**, 177206 (2015).
- [56] T. Hatomura, Shortcuts to adiabaticity in the infinite-range ising model by mean-field counter-diabatic driving, *Journal of the Physical Society of Japan* **86**, 094002 (2017).
- [57] D. Sels and A. Polkovnikov, Minimizing irreversible losses in quantum systems by local counterdiabatic driving, *Proceedings of the National Academy of Sciences* **114**, E3909 (2017).
- [58] N. N. Hegade, K. Paul, Y. Ding, M. Sanz, F. Albarrán-Arriagada, E. Solano, and X. Chen, Shortcuts to adiabaticity in digitized adiabatic quantum computing, *Phys. Rev. Appl.* **15**, 024038 (2021).
- [59] S. Yarkoni, H. Wang, A. Plaatz, and T. Bäck, Boosting quantum annealing performance using evolution strategies for annealing offsets tuning, in *Quantum Technology and Optimization Problems: First International Workshop, QTOP 2019, Munich, Germany, March 18, 2019, Proceedings 1* (Springer, 2019) pp. 157–168.
- [60] J. Côté, F. Sauvage, M. Larocca, M. Jonsson, L. Cincio, and T. Albash, Diabatic quantum annealing for the frustrated ring model, *Quantum Science and Technology* **8**, 045033 (2023).
- [61] J. Finžgar, M. Schuetz, J. Brubaker, H. Nishimori, and H. Katzgraber, Designing quantum annealing schedules using bayesian optimization (2023), arXiv preprint arXiv:2305.13365.
- [62] V. Choi, Minor-embedding in adiabatic quantum computation: I. the parameter setting problem, *Quantum Information Processing* **7**, 193 (2008).
- [63] V. Choi, Minor-embedding in adiabatic quantum computation: II. minor-universal graph design, *Quantum Information Processing* **10**, 343 (2011).
- [64] E. Weinberger, Correlated and uncorrelated fitness landscapes and how to tell the difference, *Biological cybernetics* **63**, 325 (1990).

- [65] A. Verma and M. Lewis, Penalty and partitioning techniques to improve performance of qubo solvers, *Discrete Optimization* **44**, 100594 (2022).
- [66] Solver Properties and Parameters, https://docs.dwavesys.com/docs/latest/doc_solver_ref.html.
- [67] E. Todorov, *Optimal control theory*, MIT press (2006).
- [68] L. T. Brady, C. L. Baldwin, A. Bapat, Y. Kharkov, and A. V. Gorshkov, Optimal protocols in quantum annealing and quantum approximate optimization algorithm problems, *Phys. Rev. Lett.* **126**, 070505 (2021).
- [69] T. Shirai and N. Togawa, Post-processing variationally scheduled quantum algorithm for constrained combinatorial optimization problems, *IEEE Transactions on Quantum Engineering* (2024).
- [70] J. Johansson, P. D. Nation, and F. Nori, QuTiP: An open-source Python framework for the dynamics of open quantum systems., *Phys.Comm* **183**, 1760 (2012).
- [71] J. Johansson, P. D. Nation, and F. Nori, QuTiP 2: A Python framework for the dynamics of open quantum systems., *Phys.Comm* **184**, 1234 (2013).
- [72] S. Boixo, T. F. Rønnow, S. V. Isakov, Z. Wang, D. Wecker, D. A. Lidar, J. M. Martinis, and M. Troyer, Evidence for quantum annealing with more than one hundred qubits, *Nature physics* **10**, 218 (2014).
- [73] T. F. Rønnow, Z. Wang, J. Job, S. Boixo, S. V. Isakov, D. Wecker, J. M. Martinis, D. A. Lidar, and M. Troyer, Defining and detecting quantum speedup, *science* **345**, 420 (2014).
- [74] A. Galda, E. Gupta, J. Falla, X. Liu, D. Lykov, Y. Alexeev, and I. Safro, Similarity-based parameter transferability in the quantum approximate optimization algorithm, *Frontiers in Quantum Science and Technology* **2**, 1200975 (2023).
- [75] R. Shaydulin, P. C. Lotshaw, J. Larson, J. Ostrowski, and T. S. Humble, Parameter transfer for quantum approximate optimization of weighted maxcut, *ACM Transactions on Quantum Computing* **4**, 1 (2023).
- [76] J. Falla, Q. Langfitt, Y. Alexeev, and I. Safro, Graph representation learning for parameter transferability in quantum approximate optimization algorithm, *Quantum Machine Intelligence* **6**, 46 (2024).
- [77] T. Fujii, K. Komuro, Y. Okudaira, R. Narita, and M. Sawada, Energy landscape transformation of ising problem with invariant eigenvalues for quantum annealing, *arXiv preprint arXiv:2202.05927* (2022).
- [78] T. Fujii, K. Komuro, Y. Okudaira, and M. Sawada, Eigenvalue-invariant transformation of ising problem for anti-crossing mitigation in quantum annealing, *Journal of the Physical Society of Japan* **92**, 044001 (2023).
- [79] H. Kanai and S. Tanaka, Static and dynamic analysis of energy landscape transformation of the ising problems, in *2024 IEEE International Conference on Quantum Computing and Engineering (QCE)*, Vol. 2 (IEEE, 2024) pp. 374–375.